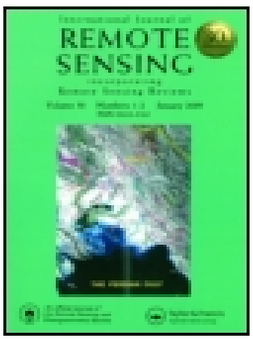

International Journal of Remote Sensing

ISSN: 0143-1161 (Print) 1366-5901 (Online) Journal homepage: https://www.tandfonline.com/loi/tres20

A nitrogen spectral response model and nitrogen estimation of summer maize during the entire growth period

Xiaobin Xu, Hongchun Zhu, Zhenhai Li, Jianwen Wang & Guijun Yang

To cite this article: Xiaobin Xu, Hongchun Zhu, Zhenhai Li, Jianwen Wang & Guijun Yang (2019): A nitrogen spectral response model and nitrogen estimation of summer maize during the entire growth period, International Journal of Remote Sensing, DOI: 10.1080/01431161.2019.1677967

To link to this article: https://doi.org/10.1080/01431161.2019.1677967

Published online: 27 Oct 2019.

INTERNATIONAL JOURNAL OF REMOTE SENSING
https://doi.org/10.1080/01431161.2019.1677967

A nitrogen spectral response model and nitrogen estimation of summer maize during the entire growth period

Xiaobin Xu[a,b], Hongchun Zhu[b], Zhenhai Li[a], Jianwen Wang[a,b] and Guijun Yang[a]

[a]Key Laboratory of Quantitative Remote Sensing in Agriculture of Ministry of Agriculture and Rural Affairs P. R. China, Beijing Research Center for Information Technology in Agriculture, Beijing, China; [b]College of Geomatics, Shandong University of Science and Technology, Qingdao, Shandong, China

ABSTRACT

Timely and effective prediction of nitrogen content in summer maize could provide support data for precise fertilization. In this study, the feasibility and expansibility of predicting the nitrogen mechanism model of summer maize leaves through its entire growth period were investigated on the basis of the theory of leaf radiation transmission mechanism. A complete random test of data from two maize varieties and two nitrogen fertilizer applications in 2017 was conducted. Three versions of the leaf optical PROperties SPECTra (PROSPECT) model, namely, PROSPECT-4, PROSPECT-5, and PROSPECT-D were used to link the established leaf nitrogen density (LND) and chlorophyll-*a* + *b* (chl-*a* + *b*) models, that is, chl-*a* + *b*-LND model. A nitrogen response transfer model (N-RTM) was established by linking the optimal PROSPECT and chl-*a* + *b*-LND models. Results were as follows. (1) chl-*a* + *b* estimation using the PROSPECT-D model yielded the highest accuracy (the coefficient of determination (R^2) = 0.774, the normalized root mean squared error (nRMSE) = 13.19%) among the three PROSPECT models, it shows that the model considering more factors can better reflect the internal law of blade, and could be used as the basic model of N-RTM; (2) Established chl-*a* + *b*-LND models based on the dataset from each growth stage showed differences using the confidence interval method, and the R^2 values of the optimal regression model at V12, VT, and R3 were 0.794, 0.781, and 0.821, respectively. Based on the changes of chl-*a* + *b* and LND during the growth period, a piecewise model was constructed; (3) The R^2 and nRMSE values between the measured and estimated LNDs were 0.656% and 22.86%, respectively. The validation results are better than the traditional empirical model. The results showed that the segmented model, which considered the interaction of various factors within the leaves and the change of chl-*a* + *b*-LND during the growth period, had better performance in nitrogen monitoring. The constructed nitrogen model in this study preliminarily realized the remote sensing prediction of the nitrogen mechanism model and had a certain mechanism.

ARTICLE HISTORY
Received 15 October 2018
Accepted 27 July 2019

CONTACT Zhenhai Li lizh323@126.com Key Laboratory of Quantitative Remote Sensing in Agriculture of Ministry of Agriculture P. R. China, Beijing Research Center for Information Technology in Agriculture, Beijing 100097, China

1. Introduction

Nitrogen is the most important element in maize, which is especially sensitive to nitrogen fertilizer (Chen et al. 1992; Wang et al. 1992). A reasonable nitrogen supply is the key for controlling maize growth and development, improving photosynthetic performance, and increasing yield (Li, Liu, and Zhou et al. 2002; Jun, Gao, and Wang et al. 2011; He et al. 1998). Under the action of electromagnetic wave, matter will produce spectral absorption and reflection characteristics, which manifest the information of material composition and structure in a specific wave band. These absorption and reflection characteristics are usually referred to as spectral characteristics, which are the bases for detecting physical and chemical compositions of various substances via remote sensing (Yang et al. 2015). The key to the diagnosis of nitrogen via remote sensing is to determine the nitrogen content of maize across different growth stages using its spectral characteristics (e.g. vegetation indices and spectral absorption features). Moreover, the demand for rapid spatial and temporal induction of maize nitrogen is also the key driving force of precision agriculture.

The estimation of plant leaf biochemical components based on hyperspectral remote sensing with a combing of spectral analysis techniques is an efficient method for the rapid acquisition of plant biochemical component information in large regions (Lv et al. 2012). Predecessors have established a functional relationship between the spectral curves of various integrated features of plant leaves and nitrogen content (Zhang 2015), and these spectral features have been used directly to reflect leaf nitrogen content (LNC). Kokaly and Clark (1999) studied the spectral absorption characteristics of 2056, 2076, and 2168 nm to estimate the nitrogen content of rice leaves. Niu, Chen, and Sui et al. (2000) found that the first derivative of spectral reflectance at 2120 nm and 1120 nm is highly correlated with the nitrogen content of fresh leaves. Feng et al. (2008) showed that the red edge and its area parameters (REPIE, $SD_r - SD_b$, and FD729) are closely related to LNC. Zhang et al. (2013) analysed the relationship between continuum removal curves, valley depth, and logarithmic changes and LNC of a mangrove. In the past few decades, spectral indices sensitive to plant nitrogen status were constructed, and LNC was estimated on the basis of spectral indices (Gitelson, Gritz, and Merzlyak 2003; Reyniers et al. 2006; Noh et al. 2012; Schlemmer et al. 2013). Chen et al. (2010) proposed a double-peak canopy nitrogen index sensitive to plant nitrogen content based on the bimodal characteristics of the red edge location. Feng et al. (2016) constructed a water resistance nitrogen index, which eliminated the influence of moisture on LNC during fertility and improved the accuracy of LNC inversion. Although the predecessors built many models on the relationships between nitrogen and spectrum, they mainly focused on extracting sensitive spectral characteristics or screening sensitive vegetation index. And these models are mostly relationships or empirical models established under specific environmental conditions, lacking versatility (John 1987). Moreover, research on a nitrogen-based radiation transport mechanism has rarely been reported. Therefore, a nitrogen radiation response model with strong mechanism must be constructed.

Numerous studies have shown a close relationship between nitrogen and chlorophyll-*a* + *b* (chl-*a* + *b*) contents (Evans 1983). Evans et al. (1989) showed that the thylakoid nitrogen content is directly proportional to the chl-*a* + *b* content. Wullschleger et al. (1993) and Baret and Buis (2008) found a close relationship between chl-*a* + *b* and nitrogen contents in maize leaves, and between nitrogen content and crop yield.

Further studies have shown that chl-*a* + *b* is dominant in spectral radiation transmission. Therefore, chl-*a* + *b* provides the necessary link between spectral features and nitrogen (Zarco-Tejada et al. 2002a; Boegh et al. 2002; Zhu et al. 2008; Glenn, Daniel, and Garry 2010). Jacquemoud and Baret (1990) proposed the chl-*a* + *b*-based radiation transmission model PROperties SPECTra (PROSPECT), which can accurately simulate the hemispherical reflectivity and transmittance of different plant leaves (i.e. monocotyledonous, dicotyledonous, and old leaves) from 400 nm to 2500 nm. After the unremitting research, PROSPECT-2 (Fourty, Baret, and Jacquemoud 1996), PROSPECT-3 (Jacquemoud et al. 1996), PROSPECT-4, PROSPECT-5 (Féret et al. 2008), and PROSPECT-D (Féret et al. 2017) were introduced one after another. The present study was based on the latest PROSPECT-4, PROSPECT-5, and PROSPECT-D models. In addition, crop nitrogen uptake and distribution theory suggest that plant nitrogen concentrations monotonically decrease with crop growth during the vegetative growth period of crops (Lemaire, Jeuffroy, and Gastal 2008). However, there is a need to determine whether the relationship between chl-*a* + *b* and nitrogen in maize is stable across different growth periods.

Therefore, in this study, (1) three versions of the PROSPECT models (PROSPECT-4, PROSPECT-5 and PROSPECT-D) were selected, and the optimal PROSPECT model was selected based on the inverted chl-*a* + *b* content; (2) the correlation between the chl-*a* + *b* and nitrogen of summer maize in different growth stages was analysed, and the chl-*a* + *b*–leaf nitrogen density (LND) model was constructed; (3) a cross-test method was used to validate the differences of chl-*a* + *b*-LND models at each growth period; and (4) the nitrogen response transfer model (N-RTM) integrated by the optimal PROSPECT model and the chl-*a* + *b*-LND model was constructed to estimate the LND of maize.

2. Materials and methods

2.1. Field experiments

A field experiment was conducted in Xiaotangshan National Precision Agriculture Research and Demonstration Base (40°00′–40°21′N, 116°34′–117°00′E, and 36 m), Changping District, Beijing, China. The base has a temperate monsoon semi-humid climate with an annual average temperature of 11.8°C and an annual average precipitation of 550.3 mm (mainly concentrated in summer). The test variables included various cultivars and different nitrogen fertilization rates. Experiment (Exp.) 1 was performed in 2013 as a completely randomized design with three replications of one maize cultivar (Zhengdan958) and four urea fertilizer application rates (0, 131.25, 262.5, and 525 kg ha^{-1}). Exp. 2 was designed in 2017 as a completely randomized design with two maize cultivars (Jingke968 and Zhengdan958) and two urea fertilizer application rates (0 kg ha^{-1} and 420 kg ha^{-1}). Other management procedures, such as pest management, weed control, and phosphate and potassium fertilizers, followed local standard practices for maize production.

2.2. Data acquisition

In agriculture, due to the results of quantitative and qualitative changes and the impact of environmental changes, there are different stages of changes in both external morphological characteristics and internal physiological characteristics. These stages of change are called

growth periods. The sampling time in this study were in the corresponding stages of maize growth. In the growth stages of V12 and VT in 2013 and V12, VT and R3 in 2017, a whole representative plant was selected from each plot and was brought back to the laboratory, and the stems and leaves were then separated. In Exp.1, each two adjacent-expanded leaves of the plant were classified into one sample. To ensure the integrity of leaves, only two samples were taken from each maize plant in V12, in other words, the first four adjacent fully unfolded leaves from top to bottom. At VT, four samples were taken from each maize plant, in other words, the first eight adjacent fully unfolded leaves from top to bottom. In Exp.2, each adjacent fully expanded leaf of the plant was taken as a sample. In all the measurements of the two experiments, including spectra, chlorophyll and nitrogen, were one-to-one correspondence. Table 1 shows a detailed introduction about data collection.

2.2.1. Determination of leaf spectrum

Leaf spectral measurements were taken using a FieldSpec FR2500 spectroradiometer coupled with an ASD Leaf Clip (Analytical Spectral Devices Inc., Boulder, Colorado, USA). The spectral range was 350–2500 nm, the resolutions of which were 1.4 nm and 2 nm in the ranges of 350–1000 nm and 1000–2500 nm, respectively. The spectral resampling interval was 1 nm. During measurement, the ASD Leaf Clip clamps the central position of the vein. The mean of the four reflectance curves was taken as the leaf reflectance spectrum curve, and that of the other four transmittance curves was taken as the leaf transmittance spectrum curve.

2.2.2. Acquisition of agronomic parameters

The position of the sample spectrum was determined, and the chl-a + b value was measured using a Dualex 4 nitrogen balance index metre (Force-A, Orsay, France). A paper bag containing the sample was placed in the oven, with temperature set to 105°C for 30 min. The temperature was then adjusted to 80°C, and the sample was dried to a constant weight (approximately 24–48 h). Finally, the total nitrogen content of the LNC in summer maize was determined using Buchi B-339 (Bucih, Flawil, Switzerland). The calculation methods of equivalent water thickness C_w (the unit is cm), dry matter content C_m (the unit is g cm^{-2}), and LND (the unit is g cm^{-2}) are discussed as follows.

$$C_w = \frac{W_F - W_D}{A_L} \times 100\%$$

$$C_m = \frac{W_D}{A_L}$$

$$\mathrm{LND} = \mathrm{LNC} \times C_m \times 1000 \quad (1)$$

Table 1. Summary of maize samples during 2013 and 2017 growing season.

Date	Growth period	Number of samples	Number of unfolded blades			
15 August 2013	V12	24#	12 × 2			
27 August 2013	VT	48	12 × 4			
6 August 2017	V12	37	9	8	11	9
17 August 2017	VT	47	12	10	13	12
31 August 2017	R3	39	12	8	10	9

Note: # indicated that the complete leaves in the intermediate layer of each maize plant were collected at the time of sampling to ensure the integrity of the sample.

where W_F is the fresh weight of the leaves and the unit is g; W_D is the dry weight of the leaves and the unit is g; A_L is the leaf area and the unit is cm^2; LNC is the leaf nitrogen content and the unit is mg g^{-1}.

2.3. Methods

In this study, nitrogen spectral response model and nitrogen estimation of summer maize during the entire growth periods were constructed and specific steps (Figure 1) was as follows:

(1) Three PROSPECT models, namely, PROSPECT-4, PROSPECT-5, and PROSPECT-D (Section 2.3.1) were compared by estimating chl-*a* + *b* with the gradient descent inversion algorithm (Section 2.3.3), and the optimal PROSPECT model was selected for the construction of an N-RTM model.
(2) The chl-*a* + *b*-LND model is established. The chl-*a* + *b*-LND models of different growth stages were constructed by using the measured data in 2017. Coupled with the selected PROSPECT model, the LND of each growth period was estimated.
(3) The confidence interval method (Section 2.4.2) was used to determine whether the chl-*a* + *b*-LND relationships in different growth periods were the same. If their relationship was the same, the chl-*a* + *b*-LND model of the entire growth period was used as the N-RTM; otherwise, a subsection N-RTM was constructed, in which the LND was inverted.
(4) Model validation based on the data collected from the 2013 growing season was evaluated in this study.

2.3.1. Gradient descent inversion algorithm

The gradient descent algorithm is a commonly used iterative method, which is efficient in optimization problems. In this method, the extremum of the function was searched by the

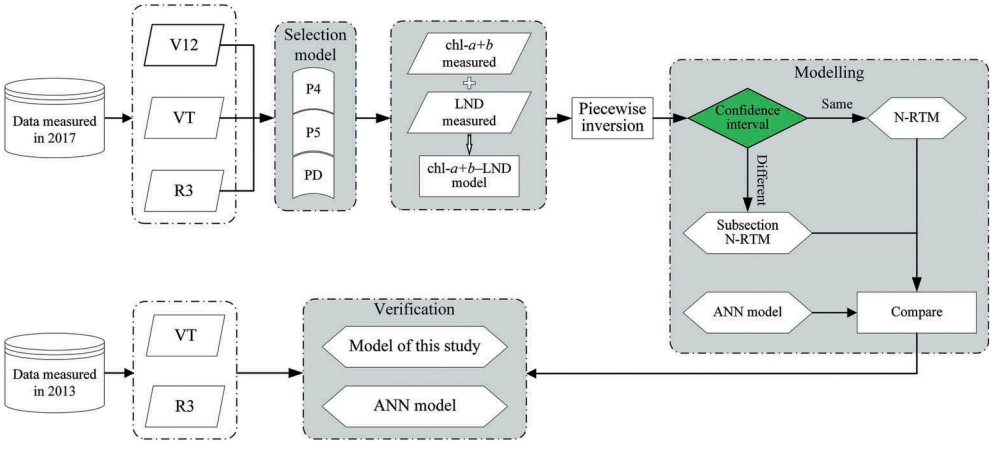

Figure 1. Flowchart of nitrogen spectral response model and nitrogen estimation across entire growth period of summer maize.

direction along the gradient. A cost function should be introduced to determine the quality of the calculation results (Guo et al. 2016).

The model variable V_a is predicted by constructing a cost function. The differences between the model-simulated and the measured spectral vegetation indices were calculated at each growth period and during the entire growth period.

$$f(V_a) = \sqrt{\frac{1}{n}\sum \left(\mathrm{VIS}_{\mathrm{prospect}} - \mathrm{VIS}_{\mathrm{leaf}}\right)^2} \quad (2)$$

where n is the number of vegetation indices selected, $\mathrm{VIS}_{\mathrm{prospect}}$ is the set of vegetation indices calculated from the spectral reflectance of the blades simulated by the PROSPECT model, and $\mathrm{VIS}_{\mathrm{leaf}}$ is the set of vegetation indices calculated from the actual-measured leaf reflectance.

The interior point minimization algorithm (Byrd, Gilbert, and Nocedal 2000) was used to minimize $f(V_a)$ by keeping the variables within their bounds (Table 2). Three initial guesses (Table 2) were used to avoid the algorithm to be trapped in a local minimum, and these guesses were set following the method of Jiang et al. (2018). The estimated biochemical contents were then calculated as the mean value over the three optimization results. The three initial guesses provided nearly the same solution in most situations.

2.3.2. Leaf spectral radiation transfer model (PROSPECT)

The PROSPECT model is a radiation transfer model used to calculate the hemispherical reflectivity and transmittance of one blade (Cheng et al. 2013). The model can simulate the optical properties of plant leaves from 400 nm to 2500 nm. The original PROSPECT-1 model was proposed by Jacquemoud and Baret (1990). The spectral absorption coefficient of this model can be expressed in formulas as follows.

$$K(\lambda) = \sum K_i(\lambda) C_i \quad (3)$$

where λ is the wavelength (400–2500 nm, step size is 1 nm), $K(\lambda)$ is the spectral absorption coefficient of the blade, $K_i(\lambda)$ is the spectral absorption coefficient of the relative leaf component i, and C_i is the content of the leaf component i per unit leaf area.

Three versions of PROSPECT, namely, PROSPECT-4 (P4), PROSPECT-5 (P5), and PROSPECT-D (PD) were used in this study (Table 3). These three versions use the following equations to calculate the effect of each blade component on spectral reflectance.

$$\begin{aligned}
K(\lambda) &= \frac{1}{N_{\mathrm{struc}}}\left[K_{\mathrm{ab}}(\lambda)\times(\mathrm{chl}-a+b)+K_{\mathrm{m}}(\lambda)\times C_{\mathrm{m}}+K_{\mathrm{w}}(\lambda)\times C_{\mathrm{w}}\right. \quad (\mathrm{P4})\\
K(\lambda) &= \frac{1}{N_{\mathrm{struc}}}[K_{\mathrm{ab}}(\lambda)\times(\mathrm{chl}-a+b)+K_{\mathrm{ar}}(\lambda)\times C_{\mathrm{ar}}+K_{\mathrm{brown}}(\lambda)\times C_{\mathrm{brown}}+K_{\mathrm{m}}(\lambda)\times C_{\mathrm{m}}+K_{\mathrm{w}}(\lambda)\\
&\quad \times C_{\mathrm{w}} \quad (\mathrm{P5})\\
K(\lambda) &= \frac{1}{N_{\mathrm{struc}}}[K_{\mathrm{ab}}(\lambda)\times(\mathrm{chl}-a+b)+K_{\mathrm{ar}}(\lambda)\times C_{\mathrm{ar}}+K_{\mathrm{ant}}(\lambda)\times C_{\mathrm{ant}}+K_{\mathrm{brown}}(\lambda)\times C_{\mathrm{brown}}+K_{\mathrm{m}}(\lambda)\\
&\quad \times C_{\mathrm{m}}+K_{\mathrm{w}}(\lambda)\times C_{\mathrm{w}}] \quad (\mathrm{PD})
\end{aligned} \quad (4)$$

where N_{struc} is the leaf structure; chl-a + b is the chlorophyll-a + b content; $K_{\mathrm{ab}}(\lambda)$ is the absorption coefficient of chl-a + b; C_{m} is the dry matter content; $K_{\mathrm{m}}(\lambda)$ is the absorption coefficient of C_{m}; C_{w} is the equivalent water thickness; $K_{\mathrm{w}}(\lambda)$ is the absorption coefficient of C_{w}; C_{ar} is the carotenoid content; $K_{\mathrm{ar}}(\lambda)$ is the absorption coefficient of C_{ar}; C_{brown} is the

Table 2. Initial guesses and bounding limits required for each model variable.

		Initial guesses			Bounds	
Variable	unit	1	2	3	Min	Max
Chlorophyll-a + b content chl-a + b	(μg cm^{-2})	20	50	80	0	140
Carotenoid content C_{ar}	(μg cm^{-2})	2	6	18	0	40
Anthocyanin content C_{ant}	(μg cm^{-2})	1	5	10	0	20
Brown pigment content C_{brown}	(μg cm^{-2})	0.001	0.010	0.200	0.000	1.000
Equivalent water thickness C_w	(cm)	0.0015	0.0050	0.0180	0.0010	0.0300
Dry matter content C_m	(g cm^{-2})	0.008	0.012	0.040	0.001	0.050
Leaf structure N_{struc}	–	1.0	1.3	1.5	1.0	1.5

Note: List of the three initial guesses and bounding limits used to minimize the cost function for each variable. Min and Max are the minimum and maximum bounding values of each variable.

brown pigment content; $K_{brown}(\lambda)$ is the absorption coefficient of C_{brown}; C_{ant} is the anthocyanin content; and K_{ant} (λ) is the absorption coefficient of C_{ant}.

2.3.3. Artificial neural network (ANN)

A neural network is a computer system formed by a plurality of very simple processing units interconnected in some manner to each other, the system processing information by its dynamic response to external input information (Lu et al. 2019). Back propagation (BP) neural network is the most representative and widely used model of artificial neural network (ANN). It has the ability of self-learning, self-organization, self-adaptation and strong non-linear mapping. It has a simple structure, good operation ability and strong structural plasticity (Wang et al. 2004). Therefore, this study chose ANN to construct an LND inversion model as a control. The 2017 data is used for modelling and the 2013 data is used for verification.

2.3.4. Vegetation index

Fourteen chl-a + b-related vegetation indices were selected on the basis of the spectral characteristics of summer maize and previous research results (Table 4), and the correlation coefficients between these vegetation indices and chl-a + b were compared. The top eight vegetation indices were screened to construct the cost function in a gradient descent inversion algorithm.

2.3.5. Statistical analysis

2.3.5.1. Accuracy evaluation. The coefficient of determination (R^2) and the normalized root mean squared error (nRMSE) were used to evaluate the pros and cons of the model.

Table 3. The input variables and abbreviations of the original model.

Version	Abbreviation	Model variable (V_a)
PROSPECT-4	P4	N_{struc} chl-a + b C_w C_m
PROSPECT-5	P5	N_{struc} chl-a + b C_{ar} C_{brown} C_w C_m
PROSPECT-D	PD	N_{struc} chl-a + b C_{ar} C_{ant} C_{brown} C_w C_m

Table 4. Vegetation index calculation formula.

VI	Name	Formula	Reference
GNDVI	Green normalized difference VI	$(R_{750}-R_{550})/(R_{750}+R_{550})$	Baret et al. 1991
$NDVI_{g\text{-}b}$	Normalized difference VI green-blue	$(R_{573}-R_{440})/(R_{573}+R_{440})$	Hansen et al.2003
MCARI	Modified chlorophyll absorption ratio index	$(R_{700}-R_{670}-0.2\times(R_{700}-R_{550}))\times(R_{700}/R_{670})$	Daughtry, Walthall, and Kim et al. 2000
MTVI2	Modification of the triangle VI 2	$\frac{1.5\times[1.2\times(R_{800}-R_{500}-2.5\times(R_{670}-R_{550}))]}{\sqrt{2\times(R_{800}+1)^2-\left[6R_{800}-5\sqrt{R_{670}}\right]-0.5}}$	Haboudane, Miller, and Pattey et al. 2004
MCARI-MTVI2	Combined index	MCARI/MTVI2	Eitel, Long, and Gessler et al. 2007
TCARI	Transformed chlorophyll absorption in reflectance index	$3\times(R_{710}-R_{680})-0.2\times(R_{700}+R_{560})\times(R_{710}/R_{680})$	Zarco-Tejada, Miller, and Tremblay et al. 2002b
mND705	Meliorate normalized difference index	$(R_{750}-R_{705})/(R_{750}+R_{705}-2R_{445})$	Sims et al. 2002
NDCI	Normalized difference chlorophyll index	$(R_{708}-R_{665})/(R_{708}+R_{665})$	Mishra et al. 2012
PPR	Plant pigment ratio	$(R_{550}-R_{450})/(R_{550}+R_{450})$	Metternicht et al. 2003
DCNI	Double-peak canopy nitrogen index	$(R_{720}-R_{700})/\frac{R_{700}-R_{670}}{(R_{720}-R_{670}+0.03)}$	Chen et al. 2010
MSAVI	Modified soil-adjusted VI	$0.5\times[2R_{800}+1-\sqrt{(2\times(R_{800}+1)^2-8\times(R_{800}-R_{670})}]$	Qi et al. 1994
NPCI	Normalized pigment chlorophyll VI	$(R_{430}-R_{680})/(R_{430}+R_{680})$	Gitelson et al. 1996
VOG2	Vogelmann red edge index 2	$(R_{734}-R_{747})/(R_{715}+R_{726})$	Zarco-Tejad et al. 2001
$NDVI_{canste}$	NDVI Canste	$(R_{760}-R_{708})/(R_{760}+R_{708})$	Steddom et al. 2003

Notes: VI represents the vegetation index.

nRMSE generally provides a significant difference limit when describing the accuracy of a model. For example, nRMSE <10% indicates no difference; 10% ≤ nRMSE <20% denotes a small difference; 20% ≤ nRMSE <30% is moderate; and nRMSE ≥30% represents a large difference (Timsina et al. 2006; Biernath et al. 2011). The formula is:

$$\mathrm{nRMSE}=\sqrt{\frac{\sum_{i=1}^{n}\left(y_i-y_j\right)^2}{n}}/\overline{y_i} \tag{5}$$

where y_i is the measured value, y_j is the predicted value, $\overline{y_i}$ is the average of the measured values, and n is the number of samples.

2.3.5.2. Confidence interval. The confidence interval estimate was based on the point estimate and provided an interval range of the population parameters (Lipschultz et al., 2000). In this study, the confidence interval method was used to test whether the chl-*a* + *b*-LND models constructed at different growth stages were the same. chl-*a* + *b*-LND models at each growth stage, namely V12, VT, and R3 were constructed to predict LND. The constructed LND model at one stage (e.g. V12) was also used to cross-validate with other growth stages (e.g. VT and R3), and three groups of predicted LND were obtained at each growth period with a total of nine LND groups. Then, the 95% confidence interval of the difference between any two groups of LNDs predicted during each growth period was calculated. If the confidence interval contains 0, then no difference between the two sets

Table 5. Correlations between vegetation indices and chl-*a* + *b* (*n* = 123).

	GNDVI	$NDVI_{g-b}$	MCARI	MTVI2	MCARI_MTVI2	TCARI	mND705
chl-*a* + *b*	0.868*	−0.821*	−0.889*	−0.690*	−0.895*	−0.904*	0.920*
	NDCI	PPR	DCNI	MSAVI	NPCI	VOG2	$NDVI_{canste}$
chl-*a* + *b*	−0.659*	−0.777*	0.855*	0.490*	0.668*	−0.929*	0.911*

Note: * represents a significance value of 0.01.

of predicted values was shown; thus, the two models are the same. Otherwise, the two models are considered different.

3. Results

3.1. PROSPECT model for chl-a + b estimation

The correlation analysis of 14 vegetation indices with chl-*a* + *b* (Table 5) showed that all selected vegetation indices demonstrated high significance ($p < 0.01$) with chl-*a* + *b*, in which the most relevant vegetation index was VOG2 ($r = -0.929$), and the worst was MSAVI ($r = 0.490$). In this study, eight vegetation indices with the highest correlation coefficient [i.e. NDVI ($r = 0.868$), MCARI ($r = -0.889$), MCARI-MTVI2 ($r = -0.895$), TCARI ($r = -0.904$), mND_{705} ($r = 0.920$), DCNI ($r = 0.855$), VOG2 ($r = -0.929$), and $NDVI_{canste}$ ($r = 0.911$)] were selected to construct the cost function of model inversion .

Three PROSPECT models (P4, P5, and PD) were used to estimate chl-*a* + *b* using the gradient descent inversion algorithm. The results (Figure 2) showed that a significant level ($p < 0.01$) of each PROSPECT model exists, with R^2 values of 0.686, 0.686, and 0.774. P4 and P5 were not ideal for predicting chl-*a* + *b* because the underestimation phenomenon was revealed at a high chl-*a* + *b* value. The nRMSE values between the measured and estimated chl-*a* + *b* via P4 and P5 were 34.47% and 33.7%, respectively. The estimated chl-*a* + *b* by the PD model yielded a significant improvement with an nRMSE value of 13.19%. The estimated and measured chl-*a* + *b* were distributed well in a 1:1 line. Therefore, the PD model was selected as the optimal model for chl-*a* + *b* estimation.

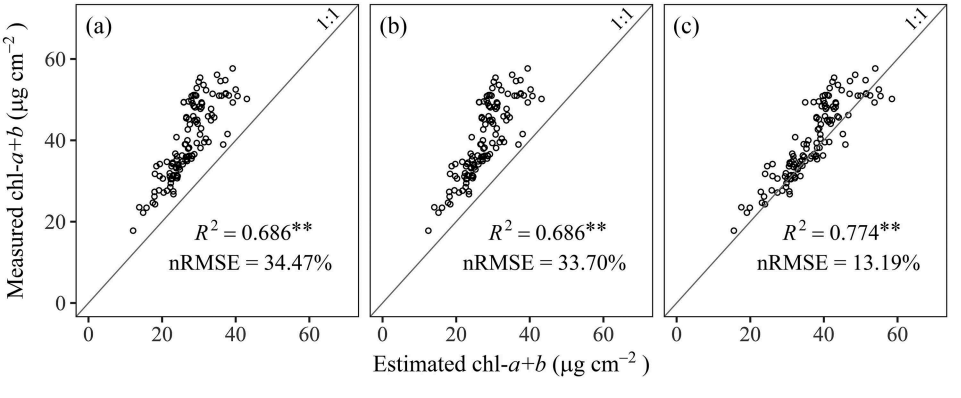

Figure 2. Comparison between measured and estimated chl-*a* + *b*.

Note: (*a*) indicative P4 model, (*b*) indicative P5 model, (*c*) indicative PD model.

3.2. Construction of chl-a + b-LND model

Correlations between LND and chl-a + b in various growth stages of maize were analysed, and regression models of LND and chl-a + b were established (Table 6). A significant difference ($p < 0.01$) was observed in each chl-a + b-LND model at each growth period. At the V12 stage, the quadratic model ($R^2 = 0.794$) between LND and chl-a + b showed higher accuracy than the other two models, whereas established exponential models at the VT and R3 stages were superior to the other two models, with R^2 values of 0.781 and 0.821, respectively.

3.3. Comparison of chl-a + b-LND in different growth stages

Figure 3 shows that any two groups of predicted LND (e.g. V12-VT for VT) were different except V12-VT for V12. Combining the nine sets of prediction results, we could not think that the three models have the same effect at any period. Therefore, an N-RTM model based on the relationship between each key growth period of chl-a + b-LND must be constructed for accurate prediction. The model is shown as follows:

$$\mathrm{LND} = \begin{cases} 0.0691 \times (\mathrm{chl} - a + b)^2 - 2.3957 \times (\mathrm{chl} - a + b) + 95.504 & \mathrm{V12} \\ 34.979\mathrm{e}^{0.0292 \times (\mathrm{chl} - a + b)} & \mathrm{VT} \\ 28.744\mathrm{e}^{0.0328 \times (\mathrm{chl} - a + b)} & \mathrm{R3} \end{cases} \quad (6)$$

3.4. LND estimation by integrating the chl-a + b-LND and PD models

The N-RTM model was constructed by combining the chl-a + b-LND and PD models. The results showed that the constructed N-RTM model considering the subsection chl-a + b-LND models yielded a significant level ($p < 0.01$), with R^2 and nRMSE values of 0.742% and 17.95%, respectively (Figure 4(a)). Moreover, the LND was estimated using the PD model linked with one chl-a + b-LND model at the entire growth stage to compare the performance of the N-RTM model, the R^2 and nRMSE values of which were 0.649% and 19.19%, respectively. The LND prediction of N-RTM during the sub-growth period is more reliable than that without considering the subsection

Table 6. Models and correlations of chl-a + b-LND at different growth stages.

Growth period	Model	Equation	R^2
V12(n = 37)	Linear model	$y = 2.908x$-0.722	0.745*
	Exponential model	$y = 40.616\mathrm{e}^{0.0253x}$	0.768*
	Quadratic model	$y = 0.0691x^2$-2.3957x+95.504	0.794*
VT(n = 47)	Linear model	$y = 3.309x$-14.886	0.771*
	Exponential model	$y = 34.979\mathrm{e}^{0.0292x}$	0.781*
	Quadratic model	$y = 0.0277x^2$ + 1.1159x+26.176	0.774*
R3(n = 39)	Linear model	$y = 3.8382x$-40.536	0.790*
	Exponential model	$y = 28.744\mathrm{e}^{0.0328x}$	0.821*
	Quadratic model	$y = 0.081x^2$-2.8339x+90.062	0.815*
All(n = 123)	Linear model	$y = 3.3434x$-17.893	0.763*
	Exponential model	$y = 34.771\mathrm{e}^{0.029x}$	0.782*
	Quadratic model	$y = 0.0667x^2$-1.9616x+82.013	0.788*

Note: * indicates the significance level $p < 0.01$.

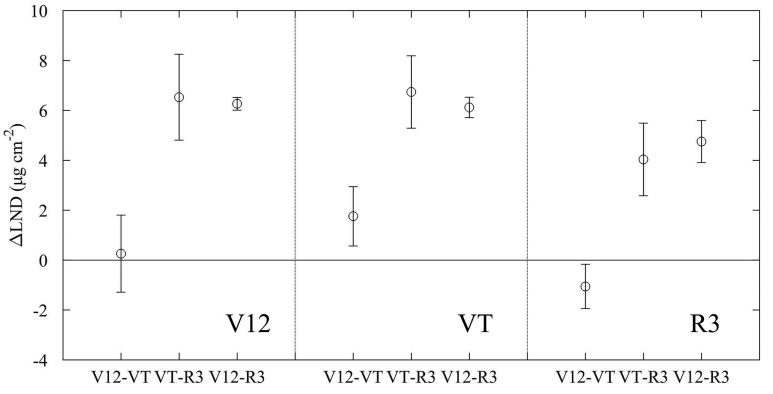

Figure 3. The difference between the two estimated LND models from different growth stages at the 95% confidence interval.

Note: In the V12 chart, V12-VT represents the average of the LND differences for each growth period for V12 and VT, respectively, and the other similarities.

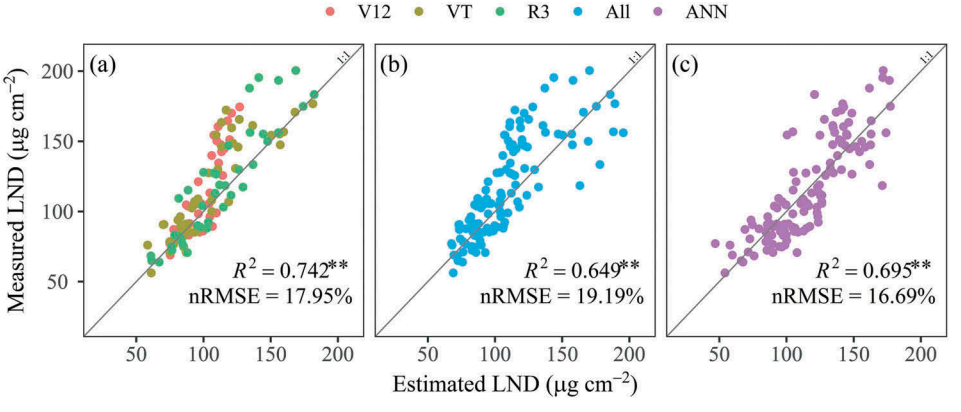

Figure 4. Comparison between measured LND and inversion LND.

Note: (*a*) the relationship between the LND inverted by the chl-*a* + *b*-LND model corresponding to the three growth stages and the measured LND; (*b*) the relationship between the LND inverted by the chl-*a* + *b*-LND model corresponding to the entire growth stage and the measured LND, and the legend 'All' represents the entire growth stage; (*c*) the relation between the LND inverted by ANN Model and the measured LND.

chl-*a* + *b*-LND model. These results proved that the relationship of chl-*a* + *b* and LND was different across different maize growth periods. In addition, the inversion accuracy of the segmentation model considering chl-*a* + *b* and LND changes is similar to that of ANN (R^2 = 0.695, nRMSE =16.69%). Therefore, the segmented N-RTM model with stronger mechanism was used to estimate LND in maize leaves.

3.5. N-RTM model verification

The dataset collected from the 2013 growing season was used to verify the reliability of the N-RTM model for LND estimation. The model accuracy reached a significant level, and the prediction result was reliable, with R^2 and nRMSE values of 0.656% and 22.96%, respectively (Figure 5(a)). However, the validation results of the ANN model were poor, with R^2 and nRMSE values of 0.267% and 26.00%, respectively (Figure 5(b)). It indicates that the ANN model has poor inter-annual transfer, and the segmented N-RTM model can effectively avoid this problem. The results of LND prediction based on the models established in each growth period could provide a technical basis for the potential application of remote sensing technology in detecting and diagnosing plant nitrogen nutrition in summer maize production.

4. Discussion

In this study, three versions of the PROSPECT model were compared in selection of the prior mechanism model. The PD model performed better than the P4 and P5 models in terms of chl-*a* + *b* estimation. The possible reason could be that the PD model considered more factors (e.g. carotenoid and anthocyanin), and the internal mechanism characteristic of the blade was closer to the actual situation. A sensitive analysis of the PD model on different input parameters was performed (Figure 6; Xiao et al. 2014), and the results showed that C_{ant} and C_{ar} had a strong sensitivity to spectral reflectance at wavelengths between 400 nm and 600 nm (Figure 6). These bands (e.g. 440, 550, and 573 nm) used for constructing vegetation indices were considered to construct a cost function in the inversion. The result was consistent with that obtained by Féret et al. (2017), which demonstrated that the PD model was more realistic in simulating the spectral reflectance of the blade.

To estimate the LND in summer maize accurately, the relationship between the LND and chl-*a* + *b* in each growth period was analysed, and the subsection model was established. The results showed that the accuracy of LND estimation by N-RTM during

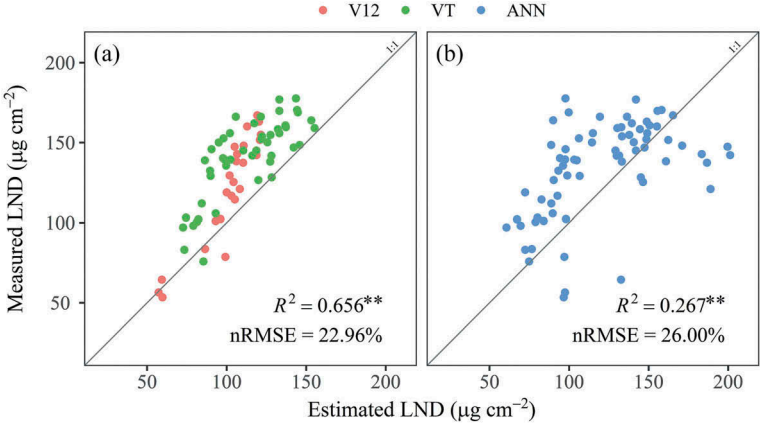

Figure 5. Comparison between measured LND and inversion LND.

Note: (*a*) represent piecewise model; (*b*) represent ANN model.

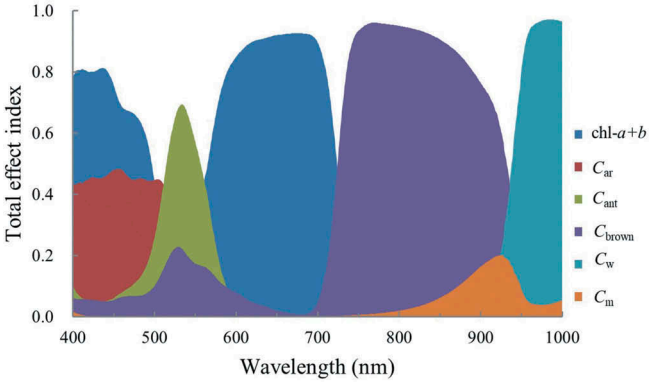

Figure 6. Sensitivity analysis of each variable in PD model.

the sub-growth period was higher than that of the entire growth period model. This result could be explained by the theory developed by Greenwood et al. (1990), which was used to explain the dilution of nitrogen in growing plants. The ratio of structural to metabolic nitrogen in leaves during corn growth was not constant (Lemaire, Jeuffroy, and Gastal 2008). The metabolism during the vegetative growth period was active, and the proportion of metabolic nitrogen associated with chl-*a* + *b* was high. As maize grew and developed, metabolism slowed down and the proportion of structural nitrogen gradually increased. The ratio of structural to metabolic nitrogen was not stable throughout the growth period, and the relationship between nitrogen content and chl-*a* + *b* was unstable.

When the N-RTM was validated with the 2013 data, although the accuracy reached a significant level, the overall performance was unsatisfactory. In the slightly high concentration of LND areas, an 'underestimation' phenomenon even occurred. The reason for this phenomenon may be that the measurement of the blade spectrum was not at the same position as that of the chl-*a* + *b* during the 2013 growing season, thereby reducing the accuracy of the inversion.

Generally, on the basis of the theory of radiation transmission mechanism combined with the relationship between chl-*a* + *b* and nitrogen, the three estimation models of summer maize are reliable and can be expanded to the interannual period. In addition, this study is the preliminary stage of a theoretical study on nitrogen space–time dynamic response. In the future, we will collect more crops and accumulate more years of samples to further verify the universality of subsection N-RTM. More intensive experiments are necessary to design and establish a comprehensive nitrogen estimation model in the entire growth period. The distribution relationship between chl-*a* + *b* and nitrogen in each growth period should be further explored. To expand the development of a more universal nitrogen estimation model, the PROSAIL model should be incorporated to design multiplatform and multiregional experiments in a regional scale. More accurate and real-time nitrogen monitoring tools were provided for large-scale agricultural planting. This study only focuses on crop development, and the model must be applied to other crops to develop a nitrogen detection model suitable for other crop varieties.

5. Conclusion

The N-RTM model, which was constructed by integrating the PROSPECT model and the physiological relationship between chl-*a* + *b* and LND, could accurately estimate LND. The main conclusions are as follows:

(1) PD performed better (R^2 = 0.774, nRMSE = 13.19%) than the P4 and P5 models.
(2) The difference of the chl-*a* + *b*-LND model in summer maize growth period was verified by calculating the confidence interval, and the subsection N-RTM was constructed.
(3) The N-RTM constructed by chl-*a* + *b*-LND was used to invert the LND of summer maize leaves with R^2 of 0.742 and nRMSE of 17.95%, which were higher than the inversion of the relationship of the entire growth period of chl-*a* + *b*-LND (R^2 = 0.649, nRMSE = 19.19%).
(4) The validated results showed that the N-RTM had good scalability and stability with R^2 of 0.656 and nRMSE of 22.96%, with an accuracy reaching a significant level.

Acknowledgements

This work was supported by the National Key Technologies of Research and Development Program (Grant No. 2016YFD0300602, 2017YFD0201501); SDUST Research Fund (Grant NO. 2019TDJH103); the Beijing Natural Science Foundation (Grant No. 6182011); Programme for Beijing Excellent Talents in Organization Department of Beijing municipal Party committee (Grant No. 2017000020060G128); the Natural Science Foundation of Beijing Academy of Agriculture and Forestry Sciences (Grant No. QNJJ201834). We also would like to thank the anonymous reviewers for providing constructive suggestions to improve the manuscript.

Disclosure statement

No potential conflict of interest was reported by the authors.

Funding

This work was supported by the Programme for Beijing Excellent Talents in Organization Department of Beijing municipal Party committee [2017000020060G128];National Key Technologies of Research and Development Program [2016YFD0300602,2017YFD0201501];SDUST Research Fund [2019TDJH103]; Beijing Natural Science Foundation [6182011];Natural Science Foundation of Beijing Academy of Agriculture and Forestry Sciences [QNJJ201834].

References

Baret, F., and S. Buis. 2008. *Estimating Canopy Characteristics from Remote Sensing Observations: Review of Methods and Associated problems[M]//Advances in Land Remote Sensing*, 173–201. Dordrecht: Springer.

Baret, F., and G. Guyot. 1991. "Potentials and Limits of Vegetation Indices for LAI and APAR assessment[J]." *Remote Sensing of Environment* 35 (2–3): 161–173. doi:10.1016/0034-4257(91)90009-U.

Biernath C., S. Gayler, S. Bittner, C. Klein, P. Högy, A. Fangmeier, and E. Priesack 2011. "Evaluating the ability of four crop models to predict different environmental impacts on spring wheat grown in open-top chambers[J]." *European Journal of Agronomy* 35(2): 71–82.

Boegh E., H. Soegaard, N. Broge, C. B. Hasager, N. O. Jensen, K. Schelde, and A. Thomsen 2002. "Airborne multispectral data for quantifying leaf area index, nitrogen concentration, and photosynthetic efficiency in agriculture[J]." *Remote Sensing of Environment* 81(2):179–193.

Byrd, R. H., J. C. Gilbert, and J. Nocedal. 2000. "A Trust Region Method Based on Interior Point Techniques for Nonlinear programming[J]." *Mathematical Programming* 89 (1): 149–185. doi:10.1007/PL00011391.

Chen, P. F., D. Haboudane, N. Tremblay, J. Wang, P. Vigneault, and B. Li. 2010. "New Spectral Indicator Assessing the Efficiency of Crop Nitrogen Treatment in Corn and wheat[J]." *Remote Sensing of Environment* 114 (9): 1987–1997. doi:10.1016/j.rse.2010.04.006.

Cheng, L. U., S. B. Chen et al. 2013. "Research of PROSPECT Leaf Optical Property model[J]." *Global Geology* 32 (01): 177–188.

Daughtry, C. S. T., C. L. Walthall, M. S. Kim, E. B. De Colstoun, and J. E. McMurtrey Iii. 2000. "Estimating Corn Leaf Chlorophyll Concentration from Leaf and Canopy Reflectance[J]." *Remote Sensing of Environment* 74 (2): 229–239. doi:10.1016/S0034-4257(00)00113-9.

Eitel, J. U. H., D. S. Long, P. E. Gessler, and A.M.S. Smith. 2007. "Using In-situ Measurements to Evaluate the New RapidEye™ Satellite Series for Prediction of Wheat Nitrogen status[J]." *International Journal of Remote Sensing* 28 (18): 4183–4190. doi:10.1080/01431160701422213.

Evans, J. R. 1983. "Nitrogen and Photosynthesis in the Flag Leaf of Wheat (triticum Aestivum L.)[J]." *Plant Physiology* 72 (2): 297–302. doi:10.1104/pp.72.2.297.

Evans, J. R. 1989. "Photosynthesis and Nitrogen Relationships in Leaves of C3 plants[J]." *Oecologia* 78 (1): 9–19. doi:10.1007/BF00377192.

Feng, W., H. Y. Zhang, Y. S. Zhang, S.-L. Qi, Y.-R. Heng, -B.-B. Guo, D.-Y. Ma, and T.-C. Guo. 2016. "Remote Detection of Canopy Leaf Nitrogen Concentration in Winter Wheat by Using Water Resistance Vegetation Indices from In-situ Hyperspectral data[J]." *Field Crops Research* 198: 238–246. doi:10.1016/j.fcr.2016.08.023.

Féret, J. B., C. François, G. P. Asner, A. A. Gitelson, R. E. Martin, L. P. R. Bidel, S. L. Ustin, G. le Maire, and S. Jacquemoud. 2008. "PROSPECT-4 and 5: Advances in the Leaf Optical Properties Model Separating Photosynthetic pigments[J]." *Remote Sensing of Environment* 112 (6): 3030–3043. doi:10.1016/j.rse.2008.02.012.

Féret, J. B., A. A. Gitelson, S. D. Noble, and S. Jacquemoud. 2017. "PROSPECT-D: Towards Modeling Leaf Optical Properties through a Complete lifecycle[J]." *Remote Sensing of Environment* 193: 204–215. doi:10.1016/j.rse.2017.03.004.

Fourty, T., F. Baret, and S. Jacquemoud. 1996. "Leaf Optical Properties with Explicit Description of Its Biochemical Composition: Direct and Inverse Problems[J]." *Remote Sensing of Environment* 56 (2): 104–117. doi:10.1016/0034-4257(95)00234-0.

Gitelson, A. A., Y. Gritz, and M. N. Merzlyak. 2003. "Relationships between Leaf Chlorophyll Content and Spectral Reflectance and Algorithms for Non-destructive Chlorophyll Assessment in Higher Plant leaves[J]." *Journal of Plant Physiology* 160 (3): 271–282. doi:10.1078/0176-1617-00887.

Gitelson, A. A., and M. N. Merzlyak. 1996. "Signature Analysis of Leaf Reflectance Spectra: Algorithm Development for Remote Sensing of Chlorophyll[J]." *Journal of Plant Physiology* 148 (s 3–4): 494–500. doi:10.1016/S0176-1617(96)80284-7.

Glenn, F., R. Daniel, and O. Garry. 2010. "Measuring and Predicting Canopy Nitrogen Nutrition in Wheat Using a Spectral Index—The Canopy Chlorophyll Content Index (CCCI)[J]." *Field Crops Research* 116 (3): 318–324. doi:10.1016/j.fcr.2010.01.010.

Greenwood, D. J., G. Lemaire, G. Gosse, P. Cruz, A. Draycott, and J. J. Neeteson. 1990. "Decline in Percentage N of C3 and C4 Crops with Increasing Plant mass[J]." *Annals of Botany* 66 (4): 425–436. doi:10.1093/oxfordjournals.aob.a088044.

Guoping, C. 1992. "Mineral Nutrition and Fertilization in Maize (review)[j]." *Maize Science* 1992(00): 59–66.

Haboudane, D., J. R. Miller, E. Pattey, P. J. Zarco-Tejada, and I. B. Strachan. 2004. "Hyperspectral Vegetation Indices and Novel Algorithms for Predicting Green LAI of Crop Canopies: Modeling

and Validation in the Context of Precision agriculture[J]." *.remote Sensing of Environment* 90 (3): 337–352. doi:10.1016/j.rse.2003.12.013.

Hansen, P. M., and J. K. Schjoerring. 2003. "Reflectance Measurement of Canopy Biomass and Nitrogen Status in Wheat Crops Using Normalized Difference Vegetation Indices and Partial Least Squares regression[J]." *Remote Sensing of Environment* 86 (4): 542–553. doi:10.1016/S0034-4257(03)00131-7.

He, P., and J. Y. Jin. 1998. "Study Progress on Maize High Yield Fertilization and Nutrition physiological[J]." *Journal of Maize Science* 6 (2): 72–76.

Jacquemoud, S., and F. Baret. 1990. "PROSPECT: A Model of Leaf Optical Properties spectra[J]." *Remote Sensing of Environment* 34 (2): 75–91. doi:10.1016/0034-4257(90)90100-Z.

Jacquemoud, S., S. L. Ustin, J. Verdebout, G. Schmuck, G. Andreoli, and B. Hosgood. 1996. "Estimating Leaf Biochemistry Using the PROSPECT Leaf Optical Properties model[J]." *Remote Sensing of Environment* 56 (3): 194–202. doi:10.1016/0034-4257(95)00238-3.

Jensen, J. R., and K. Lulla. 1987. "Introductory Digital Image Processing: A Remote Sensing perspective[J]." *Geocarto International* 2 (1). doi:10.1080/10106048709354084.

Jiang, J., A. Comar, P. Burger, P. Bancal, M. Weiss, and F. Baret. 2018. "Estimation of Leaf Traits from Reflectance Measurements: Comparison between Methods Based on Vegetation Indices and Several Versions of the PROSPECT model[J]." *Plant Methods* 14 (1): 23. doi:10.1186/s13007-018-0291-x.

Jie, L. 2012. *Hyperspectral Inversion Model of Crop Chlorophyll Content Based on Machine Learning and Radiation Transfer Model[D]*. Beijing: China University of Geosciences.

Jun, Y. E., J. L. Gao, Z. G. Wang et al. 2011. "Effects of Nitrogen on Leaf Photosynthesis and Grain Yield of Super High-yield Spring Maize during the Flowering and Milking Stages[J]." *Journal of Maize Sciences* 19 (06): 74–77.

Kokaly, R. F., and R. N. Clark. 1999. "Spectroscopic Determination of Leaf Biochemistry Using Band-Depth Analysis of Absorption Features and Stepwise Multiple Linear Regression[J]." *Remote Sensing of Environment* 67 (3): 267–287. doi:10.1016/S0034-4257(98)00084-4.

Lemaire, G., M. H. Jeuffroy, and F. Gastal. 2008. "Diagnosis Tool for Plant and Crop N Status in Vegetative Stage: Theory and Practices for Crop N management[J]." *European Journal of Agronomy* 28 (4): 614–624. doi:10.1016/j.eja.2008.01.005.

Li, C., K. Liu, S. Zhou et al. 2002. "Response of Photosynthesis to Eco-physiological Factors of Summer Maize on Different Fertilizer amounts[J]." *Acta Agronomica Sinica* 28 (2): 265–269.

Lipschultz, S., and M. Lipson. 2000. *Schaum's Outline of Theory and Problems of Probability[M]*. McGraw-Hill, Incorporated.

Longmei, L., Z. Mingsong, L. Hongliang, and Z. Ping. 2019. "Comparison of Artificial Neural Network and Random Forest in Regression Problems[J]." *Technology Innovation and Application*, no. 10: 31-32+36.

Metternicht, G. 2003. "Vegetation Indices Derived from High-resolution Airborne Videography for Precision Crop management[J]." *International Journal of Remote Sensing* 24 (14): 2855–2877. doi:10.1080/01431160210163074.

Mishra, S., and D. R. Mishra. 2012. "Normalized Difference Chlorophyll Index: A Novel Model for Remote Estimation of Chlorophyll-A, Concentration in Turbid Productive waters[J]." *Remote Sensing of Environment* 117 (2): 394–406. doi:10.1016/j.rse.2011.10.016.

Niu, Z., Y. H. Chen, H. Z. Sui, Q. Y. Zhang, and C. J. Zhao. 2000. "Mechanism Analysis of Leaf Biochemical Concentration by High Spectral Remote sensing[J]." *Journal of Remote Sensing* 4 (2): 125–129.

Noh, H., and Q. Zhang. 2012. "Shadow Effect on Multi-spectral Image for Detection of Nitrogen Deficiency in corn[J]." *Computers & Electronics in Agriculture* 83 (1): 52–57. doi:10.1016/j.compag.2012.01.014.

Qi, J., A. Chehbouni, A. R. Huete, Y. H. Kerr, and S. Sorooshian. 1994. "A Modified Soil Adjusted Vegetation index[J]." *Remote Sensing of Environment* 48 (2): 119–126. doi:10.1016/0034-4257(94)90134-1.

Reyniers, M., and E. Vrindts. 2006. "Measuring Wheat Nitrogen Status from Space and Ground-based platform[J]." *International Journal of Remote Sensing* 27 (3): 549–567. doi:10.1080/01431160500117907.

Schlemmer, M., A. Gitelson, J. Schepers, R. Ferguson, Y. Peng, J. Shanahan, and D. Rundquist. 2013. "Remote Estimation of Nitrogen and Chlorophyll Contents in Maize at Leaf and Canopy levels[J]." *International Journal of Applied Earth Observations & Geoinformation* 25 (1): 47–54. doi:10.1016/j.jag.2013.04.003.

Sims, D. A., and J. A. Gamon. 2002. "Relationships between Leaf Pigment Content and Spectral Reflectance across a Wide Range of Species, Leaf Structures and Developmental stages[J]." *Remote Sensing of Environment* 81 (2–3): 337–354. doi:10.1016/S0034-4257(02)00010-X.

Steddom, K., G. Heidel, D. Jones, and C. M. Rush. 2003. "Remote Detection of Rhizomania in Sugar beets[J]." *Phytopathology* 93 (6): 720. doi:10.1094/PHYTO.2003.93.6.720.

Timsina, J., and E. Humphreys. 2006. "Performance of CERES-Rice and CERES-Wheat Models in Rice–Wheat Systems: A review[J]." *Agricultural Systems* 90 (1–3): 5–31. doi:10.1016/j.agsy.2005.11.007.

Wang, Q., and C. Hu. 1992. "Effects of Nitrogen, Phosphorus and Potassium Deficiencies on the Plant Characters, Leaf Structure and Certain Physiological Properties in maize[J]." *Acta Agriculturae Boreali—sinica* 7 (1): 94–99.

Feng, W., Y. Zhu, Y.-C. Tian, C. Weixing, Y. Xia, and L. Yingxue. 2008. "Monitoring Leaf Nitrogen Accumulation with Hyper-spectral Remote Sensing in wheat[J]." *Acta Ecologica Sinica* 28 (1): 23–32. doi:10.1016/S1872-2032(08)60018-9.

Wullschleger, S. D. 1993. "Biochemical Limitations to Carbon Assimilation in C3 Plants—A Retrospective Analysis of the A/Ci Curves from 109 species[J]." *Journal of Experimental Botany* 44 (5): 907–920. doi:10.1093/jxb/44.5.907.

Xiao, Y., W. Zhao, D. Zhou, and H. Gong. 2014. "Sensitivity Analysis of Vegetation Reflectance to Biochemical and Biophysical Variables at Leaf, Canopy, and Regional Scales[J]." *IEEE Transactions on Geoscience & Remote Sensing* 52 (7): 4014–4024. doi:10.1109/TGRS.2013.2278838.

Yang, G., C. Zhao, R. Pu, H. Feng, Z. Li, H. Li, and C. Sun. 2015. "Leaf Nitrogen Spectral Reflectance Model of Winter Wheat (triticum Aestivum) Based on PROSPECT: Simulation and inversion[J]." *Journal of Applied Remote Sensing* 9 (1): 095976. doi:10.1117/1.JRS.9.095976.

Zhang, Y. 2015. *Multi-spectral Hyperspectral Quantitative Remote Sensing Inversion Model and Mechanism of Plant Leaves Based on PROSPECT-PLUS Model[D]*. Hangzhou: Zhejiang University.

Yihuai, W., and W. Lin. 2004. "The Nonlinear Regression Based on BP Artificial Neural Network[J]." *Computer Engineering and Applications*, no. 12: 79–82.

Yuedong, G., and S. Xudong. 2016. "Analysis and Improvement of Gradient Descent method[J]." *Technology Outlook* 26: 15.

Zarco-Tejada, P. J., and J. R. Miller. 2001. "Minimization of Shadow Effects in Forest Canopies for Chlorophyll Content Estimation Using Red Edge Optical Indices through Radiative Transfer: Implications for MERIS[C]//IGARSS 2001. Scanning the Present and Resolving the Future". *Proceedings. IEEE 2001 International Geoscience and Remote Sensing Symposium (Cat. No. 01CH37217)*, Sydney, NSW, Australia, IEEE, 2: 736–738.

Zarco-Tejada, P. J., J. R. Miller, G. H. Mohammed, T. L. Noland, and P. H. Sampson. 2002a. "Vegetation Stress Detection through Chlorophyll a + b Estimation and Fluorescence Effects on Hyperspectral imagery[J]." *Journal of Environmental Quality* 31 (5): 1433–1441. doi:10.2134/jeq2002.1433.

Zarco-Tejada, P. J., J. R. Miller, N. Tremblay, et al. 2002b. "Leaf Chlorophyll A+b and Canopy LAI Estimation in Crops Using R-T Models and Hyperspectral Reflectance Imagery[J]". *CSIC*.

Zhang, C., J. M. Kovacs, M. P. Wachowiak, and F. Flores-Verdugo. 2013. "Relationship between Hyperspectral Measurements and Mangrove Leaf Nitrogen Concentrations[J]." *Remote Sensing* 5 (2): 891–908. doi:10.3390/rs5020891.

Zhu, Y., X. Yao, Y. C. Tian, X. Liu, and W. Cao. 2008. "Analysis of Common Canopy Vegetation Indices for Indicating Leaf Nitrogen Accumulations in Wheat and rice[J]." *International Journal of Applied Earth Observation & Geoinformation* 10 (1): 1–10. doi:10.1016/j.jag.2007.02.006.